Applied Physics Letters

Weak antilocalization effect and multi-channel transport in SnTe quantum well

Cite as: Appl. Phys. Lett. **120**, 203102 (2022); https://doi.org/10.1063/5.0088499
Submitted: 17 February 2022 • Accepted: 04 May 2022 • Published Online: 17 May 2022

S. de Castro, B. Kawata, G. R. F. Lopes, et al.

Applied Physics Letters ARTICLE scitation.org/journal/apl

Weak antilocalization effect and multi-channel transport in SnTe quantum well

Cite as: Appl. Phys. Lett. **120**, 203102 (2022); doi: 10.1063/5.0088499
Submitted: 17 February 2022 · Accepted: 4 May 2022 ·
Published Online: 17 May 2022

S. de Castro,[1] B. Kawata,[2] G. R. F. Lopes,[3] P. H. de O. Rappl,[2] E. Abramof,[2] and M. L. Peres[3,a)]

AFFILIATIONS

[1]Universidade do Estado de Minas Gerais, Divinópolis, CEP 35501-170 Minas Gerais, Brazil
[2]Grupo de Pesquisa e Desenvolvimento em Materiais e Plasma, Instituto Nacional de Pesquisas Espaciais, São José dos Campos, CEP 12201-970 São Paulo, Brazil
[3]Instituto de Física e Química, Universidade Federal de Itajubá, Itajubá, CEP 37500-903 Minas Gerais, Brazil

[a)]**Author to whom correspondence should be addressed:** marcelos@unifei.edu.br

ABSTRACT

Magnetoresistance measurements were performed on a 30 nm-thick SnTe quantum well (QW) grown by molecular beam epitaxy on the BaF_2 substrate in the temperature range of 1.9–50 K. The weak antilocalization (WAL) effect was observed at low temperatures and low magnetic fields as a result of the strong spin–orbit coupling present in the QW. Using the Hikami–Larkin–Nagaoka equation, we analyzed the experimental data and found that the WAL effect is not purely 2D but composed of 2D and 3D channels that exist within the QW structure. The spin–orbit and phase coherence mechanisms are also extracted, and a general view of the transport properties of the QW is also provided.

The weak antilocalization (WAL) effect occurs due to the destruction of the interference from conducting electrons that follows a closed path in the quantum diffusive regime. This quantum interference is suppressed in the presence of the spin–orbit coupling effect that changes the phase of the electron's wave functions. In strong spin–orbit coupled systems, the WAL is an indication of metallic surface states due to a topological phase transition. The topological surface states (TSSs) of topological insulators (TIs) present massless Dirac fermions that carry a π Berry phase, leading to destructive interference of carrier wave functions, which move along a closed path, resulting in the WAL effect. To analytically verify that the WAL is due to metallic SSs, the Hikami–Larkin–Nagaoka (HLN) model is used to fit the phase coherence length as well as the number of quantum coherent channels that contribute to the electrical transport at the surface. This method is widely used for 2D and 3D WAL analysis on topological materials, such as PbSnSe,[1] SbTe,[2] BiSbTe nanoribbons,[3] $(Bi_{0.57}Sb_{0.43})_2Te_3$ nanoribbons,[4] and $Pd_3Bi_2S_2$ topological semimetal.[5]

The IV–VI binary semiconductor SnTe was predicted to have a topological crystalline insulator (TCI) phase due to its inverted band and strong spin–orbit coupling, with topological SSs that are protected by the high symmetry planes (111), (110), and (100).[6] It was experimentally confirmed that SnTe has indeed topological SSs with respect to the (111) and (110) planes, using angle-resolved photoemission spectroscopy (ARPES).[7,8] In addition, some interesting electrical properties were found, such as Shubnikov–de Haas (SdH) oscillations[9] and weak-antilocalization (WAL).[10] These effects have been reported in SnTe nanowires,[11] nanometer-thick films of SnTe grown on BaF_2 (001),[12] and on BaF_2 (111),[9] and SnTe thin films grown on the conventional TI material Bi_2Te_3.[13] The WAL analysis using the HLN model in this compound found that inter-surface and intra-surface valley scattering can couple different Dirac states, causing variations in the number of quantum coherent transport channels and the phase coherence length.[9,10,14]

In this work, the WAL effect was observed for the SnTe/$Pb_{0.90}Eu_{0.1}Te$ quantum well (QW), grown by molecular beam epitaxy (MBE) technique, at temperatures ranging from 1.9 up to 50 K. Using the HLN model, the phase-coherence length and the number of surface conduction channels were calculated, with both results showing a clear transition around 4 K. A detailed electrical characterization was also performed and magnetoresistance (MR) curves up to 9 T revealed the presence of parabolic and linear behavior in the QW. The investigation provided in this work allows a better understanding of electrical properties and the WAL effect in the SnTe QW and contributes to future investigations in SnTe based nanostructures.

The SnTe QW sample was grown on the BaF_2 (111) substrate by molecular beam epitaxy (MBE), in a Riber 32P system. The sample structure consists of a 1.5 μm $Pb_{0.9}Eu_{0.1}Te$ buffer layer followed by a 30 nm-wide SnTe layer and a 300 nm $Pb_{0.9}Eu_{0.1}Te$ cap layer [see the

schematics in Fig. 1(g)]. The reflection high-energy electron diffraction (RHEED) was used to monitor the growth process with the energy of 16 keV and 1.45 mA, was used to monitor, *in situ*, the growth process along the azimuthal direction ⟨110⟩. The electric contact preparation followed the van der Pauw geometry using gold wires soldered with indium pellets [see the inset in Fig. 1(h)]. I × V curves in Fig. 1(h) show that the contacts were Ohmic at the 1.9–10 K range. The transport properties of the sample were investigated using a Physical Property Measurement System (PPMS) from Quantum Design containing a He-cooled superconducting system with a magnetic field up to 9 T and an operating temperature of 1.9–400 K. The sample signal was detected using the standard four-probe AC lock-in technique with a constant excitation current of 10 μA.

Figures 1(a)–1(f) show the RHEED images obtained during the growth process of the $Pb_{0.9}Eu_{0.1}Te/SnTe/Pb_{0.9}Eu_{0.1}Te$ sample. Figure 1(a) shows sharp and bright diffraction dots corresponding to the growth beginning of the $Pb_{0.9}Eu_{0.1}Te$ layer, which, as expected for lead salt compounds, nucleates as islands on BaF_2 (111), especially, due to the very different chemical bonding of lead salts compared to BaF_2. Gradually, as the islands coalesce into a continuous layer, about 60 nm thick, the pattern changes to extended dots that correspond to a two-dimensional growth mode. From then on, the surface morphology is characterized with monolayer steps originated by the considerable lattice mismatch between lead salts and substrate (e.g., for PbTe, it is ∼4%) and this step flow growth mode persists to the end, as shown in Figs. 1(b)–1(f). It is particularly opportune to highlight the presence of Kikuchi lines, seen in thick layers, Figs. 1(b) and 1(f), which reveal a high crystalline perfection of the subsurface atomic layers. Finally, no reconstruction was observed.

Figure 2(a) shows the electrical resistance (R) as a function of temperature for the SnTe QW from 150 down to 1.9 K. According to this figure, it is clear that the sample exhibits a metallic behavior in the whole range of temperature. For temperatures below ∼5.0 K, the resistance drops and then slowly decreases, as can be observed in the upper inset. In this inset, we can also observe a temporary increase in $R(T)$ just before the sudden drop below 5 K. This effect is probably caused by weak localization (WL) that is suppressed by the weak anti-localization below 5 K. In the lower inset of Fig. 2(a), the first derivate of the $R(T)$ curve is shown. The arrow indicates a kink at about 86 K caused by a cubic–rhombohedral structural transition, which is close to the values found in the literature for thin films.[15,16] To investigate the drop observed in the $R(T)$ curve at low temperatures, Fig. 2(b) shows the temperature dependence of the normalized resistance (R_N) at 5 K for different magnetic fields (up to 1 T) applied perpendicularly to the sample surface [see Fig. 1(g)]. One observes that the drop observed at the zero field is completely suppressed when the magnetic field reaches 1 T. This behavior is an indication of the spin–orbit coupling effect and will be investigated later in this text. Hall measurements were also performed on the SnTe QW structure in the range of 1.9–10 K, and the temperature dependence of the carrier concentration (p) and mobility (μ) are shown in Fig. 2(c). From this figure, one observes that the carrier concentration is nearly constant while the

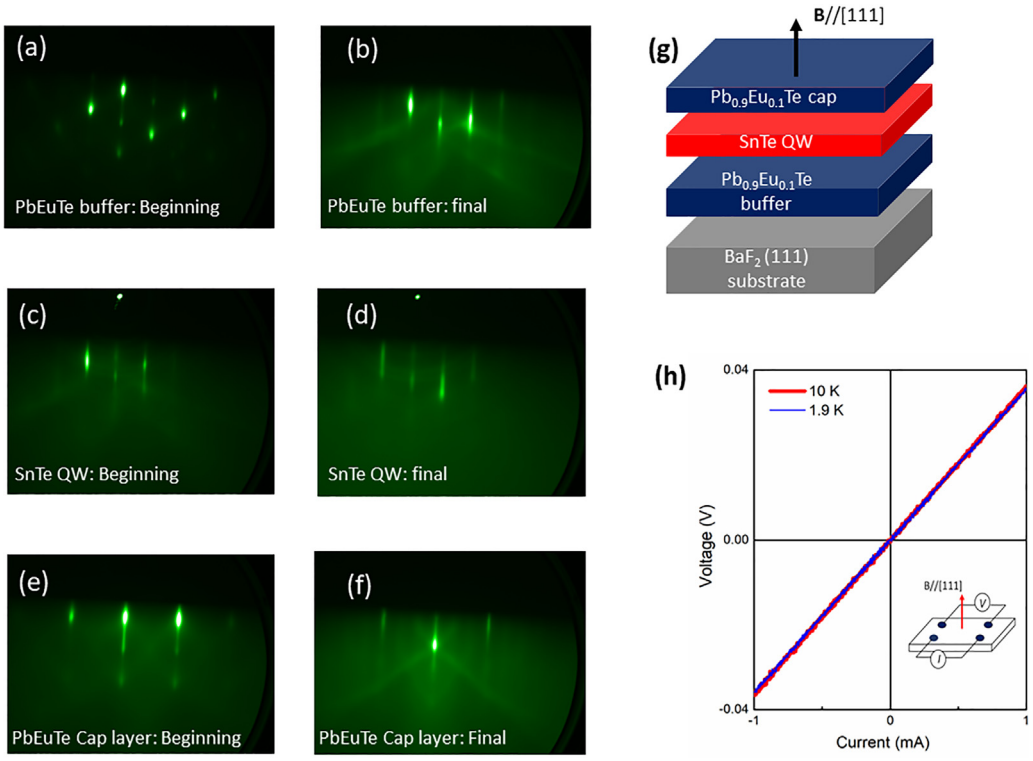

FIG. 1. (a)–(f) RHEED images taken during the growth process of the $Pb_{0.9}Eu_{0.1}Te/SnTe/Pb_{0.9}Eu_{0.1}Te$ sample on the BaF_2 substrate. The diagram of the sample structure is shown in (g) where the direction of the applied magnetic field is indicated in the direction (111). In (h), the I × V curves at 10 and 1.9 K are presented, indicating that contacts are Ohmic. The inset shows a diagram of the van der Pauw geometry used to make the contacts.

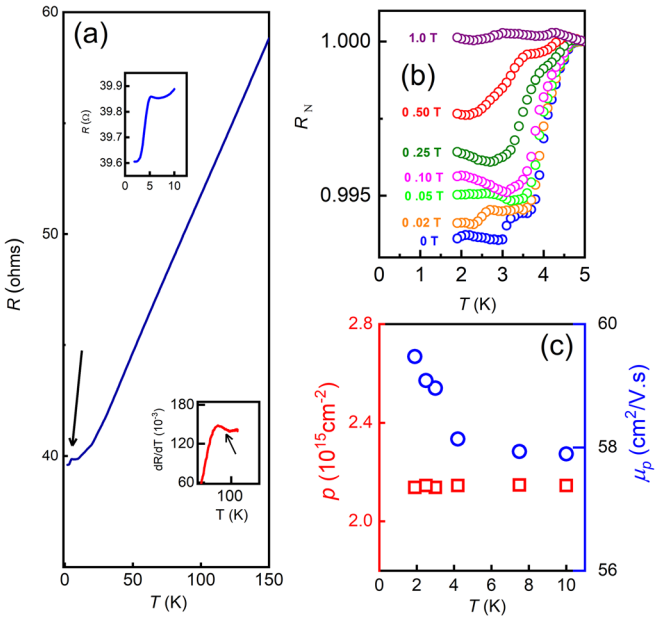

FIG. 2. (a) $R(T)$ curve for p-type SnTe QW showing metallic behavior. The lower inset displays dR_{xx}/dT as a function of temperature, where the arrow indicates the cubic–rhombohedral structural transition, and the upper inset is a zoom to clarify the R (T) curve at lower temperatures. (b) Temperature dependence of resistance under different magnetic fields (up to 1 T) applied perpendicularly to the sample surface. (c) Hall carrier concentration and mobility for the sample measured at temperatures below 10 K.

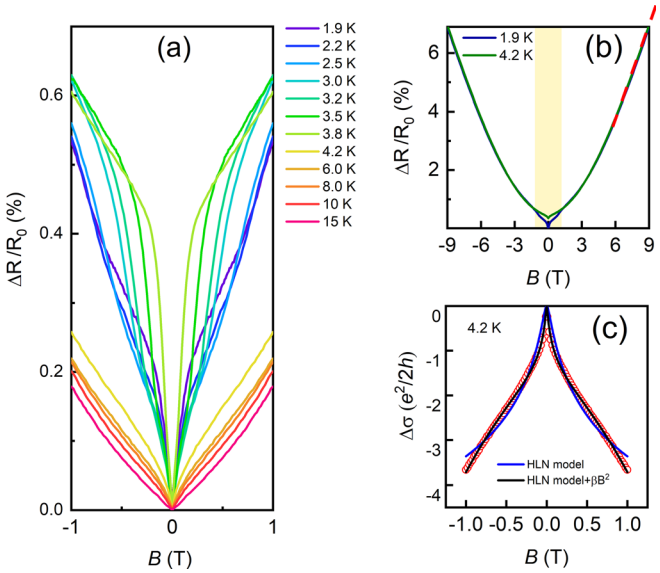

FIG. 3. Magnetoresistance ($\Delta R/R_0$) as a function of the magnetic field (a) at the range of 1.9–15 K, and (b) at 1.9 and 4.2 K for the magnetic field up to 9 T. The region with light yellow shows the MR in low fields. (c) HLN fitting to the magnetoconductivity curve at 4.2 K. The black/blue solid lines are the fits using Eq. (1) with $\beta = 0$ and β as a fitting parameters, respectively.

carrier mobility presents an evident increase when temperatures decrease below ~4 K.

To investigate the WAL effect, we performed magnetoresistance (MR) measurements on the sample. Figure 3(a) shows the MR curves plot as $\Delta R/R_0$, where R_0 is the resistance values at the zero magnetic field, for the temperature range of 1.9–15 K. At the low-field region (~0.1 T), a dip in MR is observed. As temperature increases, the dip becomes weaker as a result of the decreasing phase-coherence length. This behavior is a clear signature of WAL in the QW. However, the amplitude of the MR does not present a regular variation with temperature, i.e., the amplitude of MR due to WAL should increase as temperature decreases. Instead, one observes distinct profiles on MR curves in the different temperature regions as shown in the figure. This irregular trend in MR amplitude cannot be attributed only to the WAL effect.

WAL has been observed in various TIs at low field regions due to the π-Berry phase of the Dirac fermions that suppress the backscattering.[12,17–19] According to Assaf *et al.*,[12] the WAL in SnTe films is caused by spin-momentum locking of the TCI surface states. However, in the case of SnTe QW investigated in this work, it is not clear if the surface states survive to the disorder in the interface between the QW and the barriers, intrinsic to the growth process.

MR measurements in the sample were also carried out for fields up to 9 T for temperatures of 1.9 and 4.2 K. In Fig. 3(b), the WAL dip can be observed for both temperatures in the low-field region (light yellow area in the graph). Beyond the WAL regime, the MR exhibits a quadratic behavior followed by linear MR, for $B > 6$ T, as shown by the red dashed line, for both temperatures. Both WAL and linear MR behavior have been addressed as an indication of topological surface states contribution to electrical transport.[20–23]

To analyze the WAL observed in Fig. 3(a), we have fitted magnetoconductivity (MC) curves for different temperatures using the Hikami–Larkin–Nagaoka (HLN) model for 2D WAL in the strong spin–orbit coupling limit[24]

$$\Delta\sigma = \frac{1}{R} - \frac{1}{R_0} = -\frac{\alpha e^2}{\pi h}\left[\psi\left(\frac{\hbar}{4eL_\phi^2 B} + \frac{1}{2}\right) - \ln\left(\frac{\hbar}{4eL_\phi^2 B}\right)\right] + \beta B^2, \tag{1}$$

where R_0 is the sample resistance in zero applied magnetic field (B), ψ denotes the Digamma function, L_ϕ is the phase coherence length, which gives the average distance traveled by an electron between inelastic scattering, e and h are the electron charge and Planck's constant, respectively, and α indicates the number of 2D coherent conduction channels, which is expected to be 0.5 for each coherent diffusive transport channel. The term $\beta = \beta_q + \beta_c$ is a quadratic component. The quantum part of β (β_q) takes into account both the spin–orbit and elastic term in the HLN model and is given by

$$\beta_q B^2 = -\frac{e^2}{24\pi h}\left[\frac{B}{B_{so} + B_e}\right]^2 + \frac{3e^2}{48\pi h}\left[\frac{B}{(4/3)B_{so} + B_\phi}\right]^2 \tag{2}$$

and $\beta_c = \mu^2 B^2$ is the classical cyclotronic MR. In Eq. (2), B_e, B_ϕ, and B_{so} are the mean free path, the phase coherence, and spin coherence fields, respectively, given by $B_n = \hbar/4eL_n^2$, where $n = e, \phi, so$.

We first apply Eq. (1) to the magnetoconductivity curves of the SnTe QW measured at 4.2 K for fields up to 1 T as shown in Fig. 3(c). This figure shows that the experimental data over the entire field range

can be well fit using the HLN model with the quadratic term as a fitting parameter (see black solid line). However, for $\beta = 0$ (blue solid line) all data are not well described by Eq. (1) since at higher field regime, the elastic scattering and cyclotronic scattering term also contribute to MC.

The HLN equation for $\beta = 0$ is valid if the applied field obeys the following condition $B \ll B_{tr} = \hbar/2eL_e^2$ (B_{tr} is characteristic transport field). The elastic scattering length L_e was calculated from the transport measurements presented in Fig. 2(c), and its value is (45.74 $\pm$ 0.01) nm at 4.2 K. This value is very close to the QW thickness, which is 30 nm, indicating that the system is at the limit of 2D confinement. Furthermore, we find $B_{tr} = 0.34$ T. Hence, to precisely extract the fitting parameters, α and L_ϕ, we fitted the MC curves for fields up to 0.2 T and a temperature range of 1.9–50 K with the HLN model with $\beta = 0$ (see the supplementary material). The solid lines in Fig. 4(a) show the fitting performed, which are in good agreement with the experimental data. The fitting parameters L_ϕ and α are given in Figs. 4(b) and 4(c), respectively, where it is clear in both figures that a transition occurs at ~4 K. The phase coherence L_ϕ plotted in Fig. 4(b) shows that L_ϕ decreases with the increasing temperature following power-law behavior $L_\phi \sim T^{-0.48}$ in the temperature range of 4.2–50 K. This dependence is close to the expected behavior $T^{-0.50}$ for 2D systems, due to the electron–electron interaction,[25] which suggests that electron–electron interaction could be the dominant dephasing mechanism in the QW. The values obtained for L_ϕ from our fittings agree with the values found in the literature for SnTe films.[12,26]

In a strong spin–orbit interaction, the observation of WAL requires that the phase coherence length L_ϕ and spin–orbit scattering length L_{so} satisfy the condition $L_{so} \ll L_\phi$. To extract L_{so}, we have fitted the MC curves in Fig. 4(a) considering the quadratic component of Eq. (1) and the values of L_ϕ and L_e calculated before. From the fittings, we obtained the spin–orbit scattering length $L_{so} = (39 \pm 1)$ nm at 4.2 K. In this temperature, $L_\phi = (148 \pm 2)$ nm, which satisfies the condition $L_{so} \ll L_\phi$. As shown in Fig. 4(b), L_{so} values are nearly temperature-independent, unlike L_ϕ. In Fig. 4(c), it is possible to observe that the α values go suddenly from ~2 to ~0.7 as temperature increases beyond the critical temperature. Tanaka *et al.* performed angle-resolved photoemission spectroscopy (ARPES) measurements on the (111) surface of SnTe and observed four Dirac cones. Thus, α may lie between 0.5 and 4 for the SnTe depending on the number of participating surface states and their interaction with the bulk state. Accordingly, $\alpha = 0.5$ (4) indicates one (eight) surface channel(s) because of the combination of the top and bottom surface states of SnTe films.[8] The difference between the α values obtained experimentally and theoretical values suggests multi-parallel conduction channels (surface and bulk states).

Angular dependence of MR curves with the magnetic field allows us to distinguish the WAL effect associated with 2D states from bulk states since in a 2D transport the amplitude of the MR depends only on the perpendicular component of the applied magnetic field.[23,27–29] Therefore, to understand the origin of the WAL in the SnTe quantum well and the transition observed in Figs. 4(b) and 4(c), we performed MR measurements for different angular orientations. Figures 5(a) and 5(b) show the MR at 1.9 and 6.0 K, respectively, for different tilt angles between the magnetic field B and the sample surface direction (111) [see inset in Fig. 5(a)]. These temperatures are in different sides of the transition observed around 4.0 K. For a 2D transport only, the WAL should vanish when the angle is 90° and B is parallel to the sample surface. In both figures, (a) and (b), the amplitude of the WAL diminishes, but does not vanish completely, indicating that there is a remaining 3D component. However, it is possible to observe that the MR amplitude drops more significantly at 1.9 K than at 6.0 K when

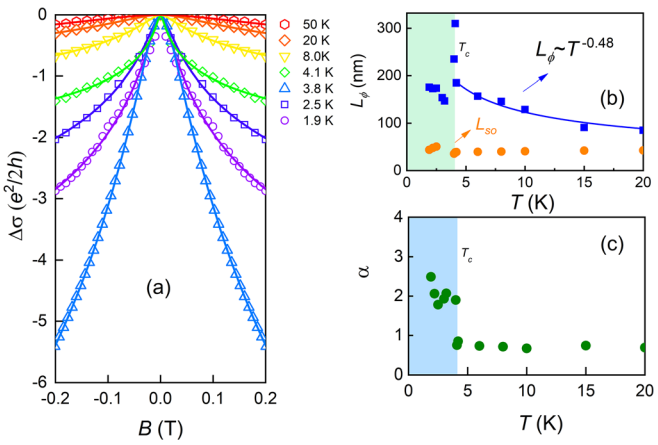

FIG. 4. (a) Magnetoconductivity curves for SnTe QW in the temperature range of 1.9–50 K, fitted using the HLN model. In (b) and (c) are the fitting parameters L_ϕ and α extracted from the HLN fit.

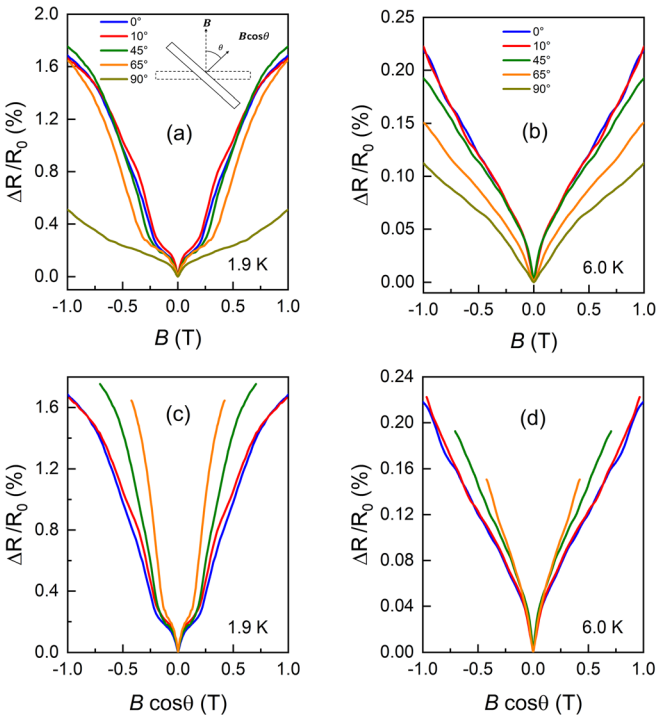

FIG. 5. (a) and (b) MR at 1.9 and 6.0 K, respectively, for different tilt angles between the magnetic field B and the sample surface direction (111) [see inset in (a)]. (c) and (d) MR as a function of $B\cos\theta$, for 1.9 and 6.0 K, respectively, where it is possible to observe that the system does not present 2D behavior.

the angle changes from 0° to 90°. If one takes the MR as a function of the perpendicular magnetic field component $B\cos\theta$, the amplitudes should overlap for all angles in the case of a 2D transport. Figures 5(c) and 5(d) present the MR as a function of $B\cos\theta$, for 1.9 and 6.0 K, respectively, where it is possible to observe that the system does not really present a pure 2D behavior as already indicated by the behavior observed in Figs. 5(a) and 5(b). In this case, the α values extracted from the HLN fit are not purely originated from 2D states, but a combination of 2D and 3D channels.

In SnTe nano-films, WAL was attributed to TSSs and the analyses of the magnetoresistance curves indicated that a coupling between all valleys (Dirac cones) was responsible for an alpha value of 0.5.[14] Also, an abrupt change in the alpha values as temperature increases around 4 K, in one of the samples, was observed and attributed to the simultaneous contribution of WAL and WL effects. On the other hand, WAL and WL effects were verified in SnTe thin-films grown on amorphous $SrTiO_3$ with different sample thickness.[26] In that case, the WL was an indication of contribution from 3D bulk states together with the 2D TSSs where bulk states were probably caused by inhomogeneity at the surfaces SnTe/$SrTiO_3$, but this statement was not conclusive. In our case, we also observed the contribution of 2D channels and 3D bulk channels. However, the origin of such channels cannot be completely elucidated. In the QW investigated in this work, the 2D channels can be originated from TSSs but also from quantum confinement of the energy levels or 2D exotic states formed at the interfaces of the QW,[13] while the presence of 3D bulk channels in our QW can be originated from broadening of subbands due to the large width of the QW. The drop of α as temperature increases is probably due to enhanced intersubband scattering that entangles the transport of subbands.[27]

In this work, we presented the investigation of the WAL effect that was observed for the 30 nm-thick SnTe/$Pb_{0.90}Eu_{0.1}Te$ quantum well, successfully grown by the molecular beam epitaxy technique. We confirmed the high quality of the sample from RHEED images obtained during the sample growth. The HLN model was used to analyze the data between 1.9 and 50 K. A clear transition is observed around 4.0 K, where the number of conduction channels increases abruptly below this temperature. For temperatures higher than 4 K, the phase coherence length showed a power-law behavior characteristic of electron–electron interaction in 2D systems, indicating that this could be the main dephasing mechanism in the quantum well sample. For the strong spin–orbit interaction, the spin–orbit coherence length showed no dependence with temperature, being much smaller than the phase coherence length and, thus, maintaining the condition for the WAL. The angular dependence on WAL showed that the sample does not present a pure 2D behavior as expected, indicating the contribution of 3D channels. In addition, comparing the quantum well thickness and the elastic scattering length, it is noted that the system is in fact within the limit of 2D confinement. Therefore, the 2D and 3D channels due to the surface and bulk states, respectively, contribute simultaneously to the electrical transport observed in the measurements. The increase in the number of channels is attributed to the enhanced intersubband scattering that entangles the transport of subbands. The abrupt change in the number of conductions channels around a critical temperature opens the possibility of the development of quantum switch devices based on SnTe QWs.

See the supplementary material for a complete description of the calculation of fitting parameters using Eqs. (1) and (2).

The authors acknowledge CAPES for its financial support.

AUTHOR DECLARATIONS

Conflict of Interest

The authors have no conflicts to disclose.

DATA AVAILABILITY

The data that support the findings of this study are available from the corresponding author upon reasonable request.

REFERENCES

[1]A. Kazakov, W. Brzezicki, T. Hyart, B. Turowski, J. Polaczyński, Z. Adamus, M. Aleszkiewicz, T. Wojciechowski, J. Z. Domagala, O. Caha, A. Varykhalov, G. Springholz, T. Wojtowicz, V. V. Volobuev, and T. Dietl, "Signatures of dephasing by mirror-symmetry breaking in weak-antilocalization magnetoresistance across the topological transition in $Pb_{1-x}Sn_xSe$," Phys. Rev. B **103**(24), 245307 (2021).
[2]S. Bera, P. Behera, A. K. Mishra, M. Krishnan, M. M. Patidar, R. Venkatesh, and V. Ganesan, "Weak antilocalization in Sb_2Te_3 nano-crystalline topological insulator," Appl. Surf. Sci. **496**, 143654 (2019).
[3]H. Li, H.-W. Wang, Y. Li, H. Zhang, S. Zhang, X.-C. Pan, B. Jia, F. Song, and J. Wang, "Quantitative analysis of weak antilocalization effect of topological surface states in topological insulator $BiSbTeSe_2$," Nano Lett. **19**(4), 2450–2455 (2019).
[4]J. Kölzer, D. Rosenbach, C. Weyrich, T. W. Schmitt, M. Schleenvoigt, A. R. Jalil, P. Schüffelgen, G. Mussler, V. E. Sacksteder IV, D. Grützmacher, H. Lüth, and T. Schäpers, "Phase-coherent loops in selectively-grown topological insulator nanoribbons," Nanotechnology **31**(32), 325001 (2020).
[5]Shama, R. K. Gopal, G. Sheet, and Y. Singh, "2D weak anti-localization in thin flims of the topological semimetal $Pd_3Bi_2S_2$," Sci. Rep. **11**(1), 12618 (2021).
[6]T. H. Hsieh, H. Lin, J. Liu, W. Duan, A. Bansil, and L. Fu, "Topological crystalline insulators in the SnTe material class," Nat. Commun. **3**(1), 982 (2012).
[7]Y. Tanaka, Z. Ren, T. Sato, K. Nakayama, S. Souma, T. Takahashi, K. Segawa, and Y. Ando, "Experimental realization of a topological crystalline insulator in SnTe," Nat. Phys. **8**(11), 800–803 (2012).
[8]Y. Tanaka, T. Shoman, K. Nakayama, S. Souma, T. Sato, T. Takahashi, M. Novak, K. Segawa, and Y. Ando, "Two types of Dirac-cone surface states on the (111) surface of the topological crystalline insulator SnTe," Phys. Rev. B **88**(23), 235126 (2013).
[9]A. K. Okazaki, S. Wiedmann, S. Pezzini, M. L. Peres, P. H. O. Rappl, and E. Abramof, "Shubnikov–de Haas oscillations in topological crystalline insulator SnTe(111) epitaxial films," Phys. Rev. B **98**(19), 195136 (2018).
[10]R. Akiyama, K. Fujisawa, R. Sakurai, and S. Kuroda, "Weak antilocalization in (111) thin films of a topological crystalline insulator SnTe," J. Phys. **568**(5), 052001 (2014).
[11]M. Safdar, Q. Wang, M. Mirza, Z. Wang, K. Xu, and J. He, "Topological surface transport properties of single-crystalline SnTe nanowire," Nano Lett. **13**(11), 5344–5349 (2013).
[12]B. A. Assaf, F. Katmis, P. Wei, B. Satpati, Z. Zhang, S. P. Bennett, V. G. Harris, J. S. Moodera, and D. Heiman, "Quantum coherent transport in SnTe topological crystalline insulator thin films," Appl. Phys. Lett. **105**(10), 102108 (2014).
[13]A. A. Taskin, F. Yang, S. Sasaki, K. Segawa, and Y. Ando, "Topological surface transport in epitaxial SnTe thin films grown on Bi_2Te_3," Phys. Rev. B **89**(12), 121302 (2014).
[14]R. Akiyama, K. Fujisawa, T. Yamaguchi, R. Ishikawa, and S. Kuroda, "Two-dimensional quantum transport of multivalley (111) surface state in topological crystalline insulator SnTe thin films," Nano Res. **9**(2), 490–498 (2016).
[15]C. D. O'Neill, D. A. Sokolov, A. Hermann, A. Bossak, C. Stock, and A. D. Huxley, "Inelastic x-ray investigation of the ferroelectric transition in SnTe," Phys. Rev. B **95**(14), 144101 (2017).

[16]C. D. O'Neill, O. J. Clark, H. D. J. Keen, F. Mazzola, I. Marković, D. A. Sokolov, A. Malekos, P. D. C. King, A. Hermann, and A. D. Huxley, "Changes of Fermi surface topology due to the rhombohedral distortion in SnTe," Phys. Rev. B **102**(15), 155132 (2020).
[17]M. Safdar, Q. Wang, Z. Wang, X. Zhan, K. Xu, F. Wang, M. Mirza, and J. He, "Weak antilocalization effect of topological crystalline insulator $Pb_{1-x}Sn_xTe$ nanowires with tunable composition and distinct {100} facets," Nano Lett. **15**(4), 2485–2490 (2015).
[18]S.-P. Chiu and J.-J. Lin, "Weak antilocalization in topological insulator Bi_2Te_3 microflakes," Phys. Rev. B **87**(3), 035122 (2013).
[19]H.-T. He, G. Wang, T. Zhang, I.-K. Sou, G. K. L. Wong, J.-N. Wang, H.-Z. Lu, S.-Q. Shen, and F.-C. Zhang, "Impurity effect on weak antilocalization in the topological insulator Bi_2Te_3," Phys. Rev. Lett. **106**(16), 166805 (2011).
[20]S. Roychowdhury, S. Ghara, S. N. Guin, A. Sundaresan, and K. Biswas, "Large linear magnetoresistance in topological crystalline insulator $Pb_{0.6}Sn_{0.4}Te$," J. Solid State Chem. **233**, 199–204 (2016).
[21]B. A. Assaf, T. Cardinal, P. Wei, F. Katmis, J. S. Moodera, and D. Heiman, "Linear magnetoresistance in topological insulator thin films: Quantum phase coherence effects at high temperatures," Appl. Phys. Lett. **102**(1), 012102 (2013).
[22]C. M. Wang and X. L. Lei, "Linear magnetoresistance on the topological surface," Phys. Rev. B **86**(3), 035442 (2012).
[23]X. Lei, L. Zhou, Z. Y. Hao, X. Z. Ma, C. Ma, Y. Q. Wang, P. B. Chen, B. C. Ye, L. Wang, F. Ye, J. N. Wang, J. W. Mei, and H. T. He, "Surface-induced linear magnetoresistance in the antiferromagnetic topological insulator $MnBi_2Te_4$," Phys. Rev. B **102**(23), 235431 (2020).
[24]S. Hikami, A. I. Larkin, and Y. Nagaoka, "Spin–orbit interaction and magnetoresistance in the two dimensional random system," Prog. Theor. Phys. **63**(2), 707–710 (1980).
[25]B. L. Altshuler, A. G. Aronov, and D. E. Khmelnitsky, "Effects of electron-electron collisions with small energy transfers on quantum localisation," J. Phys. C **15**(36), 7367–7386 (1982).
[26]S. D. Albright, K. Zou, F. J. Walker, and C. H. Ahn, "Weak antilocalization in topological crystalline insulator SnTe films deposited using amorphous seeding on $SrTiO_3$," APL Mater. **9**(11), 111106 (2021).
[27]S. Chatterjee, S. Khalid, H. S. Inbar, A. Goswami, F. C. de Lima, A. Sharan, F. P. Sabino, T. L. Brown-Heft, Y.-H. Chang, A. V. Fedorov, D. Read, A. Janotti, and C. J. Palmstrøm, "Weak antilocalization in quasi-two-dimensional electronic states of epitaxial LuSb thin films," Phys. Rev. B **99**(12), 125134 (2019).
[28]H. Tang, D. Liang, R. L. J. Qiu, and X. P. A. Gao, "Two-dimensional transport-induced linear magneto-resistance in topological insulator Bi_2Se_3 nanoribbons," ACS Nano **5**(9), 7510–7516 (2011).
[29]K. Shrestha, M. Chou, D. Graf, H. D. Yang, B. Lorenz, and C. W. Chu, "Extremely large nonsaturating magnetoresistance and ultrahigh mobility due to topological surface states in the metallic Bi_2Te_3 topological insulator," Phys. Rev. B **95**, 195113 (2017).